Acta Acustica 2022, **6**, 61
© The Author(s), Published by EDP Sciences, 2022
https://doi.org/10.1051/aacus/2022054

Available online at:
https://acta-acustica.edpsciences.org

SCIENTIFIC ARTICLE OPEN ACCESS

Characterization of acoustic materials at arbitrary incidence angle using sound field synthesis

Samuel Dupont[1], Maryna Sanalatii[2], Manuel Melon[1,*], Olivier Robin[3], Alain Berry[3], and Jean-Christophe Le Roux[2]

[1] Laboratoire d'Acoustique de l'Université du Mans (LAUM), UMR 6613, Institut d'Acoustique – Graduate School (IA-GS), CNRS, Le Mans Université, 72085 Le Mans Cedex 9, France
[2] Centre de Transfert de Technologie du Mans (CTTM), 20 Rue de Thalès de Milet, 72000 Le Mans Cedex 09, France
[3] Centre de Recherche Acoustique – Signal – Humain (CRASH), Université de Sherbrooke, 2500 Bd de l'Université, Sherbrooke, QC J1K 2R1, Canada

Received 5 August 2022, Accepted 15 November 2022

Abstract – Standardized methods for measuring sound absorption such as the impedance tube and reverberation chamber methods are limited to normal or diffuse incidence, respectively. Two research axes have been generally followed in the literature to develop alternative techniques, the first one focusing on the measurement part, that is from the two-microphone technique to the use of microphone arrays or pressure-velocity sensors. The second axis focuses on the excitation part with for instance the use of sound field synthesis techniques. Since acoustic impedance and sound absorption coefficient of materials are classically defined under normal and oblique plane wave excitation, synthesizing an "ideal" plane wave using a loudspeaker array would allow measuring these acoustics quantities using a simple microphone pair. In this article, the effect of the different parameters of a loudspeaker array on acoustic plane waves reproduction on a material's surface is first numerically studied. Then, numerical and experimental results for the estimation of both impedance and absorption coefficients are reported. These results show that sound field synthesis allows to characterize a material for arbitrary incidence angles over a wide frequency range, thus offering an alternative method to standard techniques and an improvement over existing works.

Keywords: Sound field reproduction, Free field measurement, Absorption coefficient, Acoustic impedance

1 Introduction

Acoustic comfort, noise control and reduction are important aspects of the building or transportation industries. The installation of sound absorbing materials is an effective way to reduce noise levels and thus improve the quality of the interior environment. In order to comply with the acoustic regulations when designing residential homes and workplaces, it is necessary to know the acoustic parameters of the prospective materials. Two properties of sound absorbing materials are classically used: the sound absorption coefficient and the acoustic impedance. To measure these quantities, two standardized methods exist: the impedance tube method [1, 2] and the reverberation chamber method [3, 4]. Several well-documented limitations are associated with these methods. Concerning the impedance tube, (1) it only provides results for normal incidence, (2) results are obtained on small samples that are not always representative of the global properties of the material, and (3) the upper frequency limit is restricted by the diameter of the tube [1, 2]. The reverberation chamber method provides a diffuse field absorption coefficient, which corresponds to an average value over all incidence angles. However, this method is known to produce non-physical results such as absorption coefficient values larger than unity. A minimum volume is indicated in standards, but the absence of specific dimensions for the reverberation chamber also leads to reproducibility issues between laboratories [5, 6].

The drawbacks of standardized methods have led to the development of alternative free-field measurement methods. They have focused on various topics (measurement of the sound pressure field, improvement of the sensor type, of the propagation model or of the global quality of the measurement). The best known methods use two microphones [7] or a pressure–velocity (P-U) probe [8]. Approaches using a linear microphone array have also been proposed in recent years [9, 10]. However, the measurement of material properties at low frequencies (typically below 500 Hz) and the consideration of edge effects remain challenging [11–17].

On the other hand, it is possible to generate a target acoustic field, for example a plane wave or a diffuse field, using an array of loudspeakers over an absorbing material

*Corresponding author: Manuel.Melon@univ-lemans.fr

This is an Open Access article distributed under the terms of the Creative Commons Attribution License (https://creativecommons.org/licenses/by/4.0), which permits unrestricted use, distribution, and reproduction in any medium, provided the original work is properly cited.

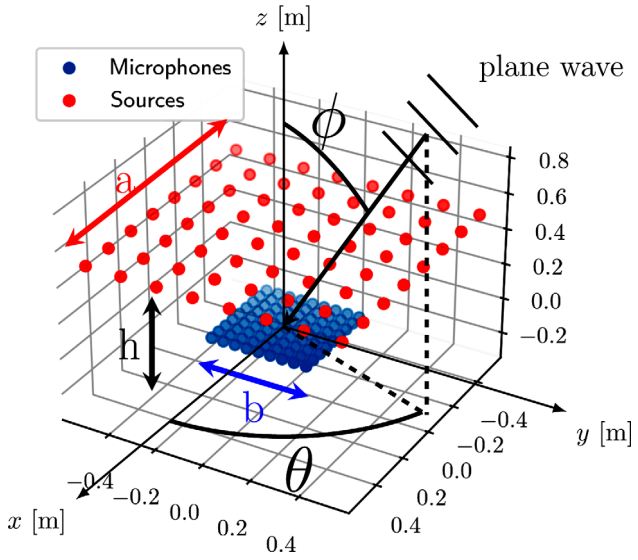

Figure 1. Configuration example of a sound synthesis system with $L = 64$ sources (in red), $a = 115$ cm and $M = 81$ microphones (in blue), $b = 40$ cm, $h = 50$ cm.

to measure its characteristics. The application of sound field reproduction methods to acoustic material characterization under a diffuse acoustic field excitation was introduced in [18–21] and in [22, 23] for normally incident plane wave.

This paper extends the work proposed in Refs. [22, 23] for measuring the acoustic impedance and sound absorption coefficient of absorbing materials, which was limited to normal incidence and was used over a reduced frequency bandwidth (250–1600 Hz). In this study, arbitrary incidence angles are considered with a targeted bandwidth of 100–4000 Hz and a material sample size of 150 × 150 cm. These specifications aim to create a more versatile and effective method for the characterization of acoustic materials. The objective is to use a material's size that is relatively small compared to the reverberation chamber requirements while characterizing a behaviour that is representative of an enlarged material sample compared to the impedance tube.

In this work, a plane wave is synthesized at different incidence angles by summing the weighted input signals of a planar array of loudspeakers located above a material to be characterized. An inverse least square method is used to determine the optimal loudspeaker signals. The reflection coefficient of the material under a synthetized plane wave is then estimated using the two-microphone technique [24].

The first part of this paper reports results from numerical simulations of a sound field synthesis method allowing the generation of plane waves at any incidence on the surface of a material to be characterized (Fig. 1). The incident and reflected parts of the reconstructed field over a porous material, and the estimated sound absorption coefficients, are all analyzed according to the loudspeaker array parameters (number of sources, source separation and height above the material). In the second part, an experimental validation is conducted using a "full" system consisting of 64 loudspeakers (Fig. 2), but also a sequential system in which a robot translates a single loudspeaker. The obtained

Figure 2. Picture showing the experimental setup, the 64-loudspeaker array being positioned above a layer of polyurethane foam.

results, and global performance of the systems are discussed as well as practical implementations.

2 Theoretical considerations

2.1 Configuration under study

A square array of side length a composed of L loudspeakers, with $\sqrt{L} \in \mathbb{N}^+$, is used to generate a plane wave of arbitrary incidence. The signals to be applied to each individual loudspeaker are computed by constraining the radiated sound pressure field on a square array of side length b sampled by M microphones, with $\sqrt{M} \in \mathbb{N}^+$. The loudspeaker and microphone arrays are parallel, separated by a distance h and their respective centers are located on the same normal to the tested material as shown in Figure 1. The microphone and source separations equal $\Delta_m = \frac{b}{\sqrt{M}-1}$ and $\Delta_l = \frac{a}{\sqrt{L}-1}$, respectively.

The sound pressure radiated by the loudspeaker l and measured by the microphone m is given by:

$$p_m(f) = g_{ml}(f) u_l(f), \tag{1}$$

where $g_{ml}(f)$ is the transfer function between microphone m and loudspeaker l (modeled as point sources in this paper, see Eq. (11)), u_l is the source strength (Pa·m) of loudspeaker l and f is the frequency. The sound pressure measured by the microphone array when all sources are active can be written in a matrix form:

$$\mathbf{p} = \mathbf{G}\mathbf{u} \tag{2}$$

with:

$$\mathbf{p} = [p_1(f), p_2(f), \ldots, p_M(f)]^T, \tag{3}$$

$$\mathbf{G} = \begin{bmatrix} g_{11}(f) & \cdots & g_{1L}(f) \\ \vdots & \cdots & \vdots \\ g_{M1}(f) & \cdots & g_{ML}(f) \end{bmatrix}, \tag{4}$$

$$\mathbf{u} = [u_1(f), u_2(f), \ldots, u_L(f)]^T. \quad (5)$$

where ^{T} denotes the transpose of a matrix.

2.2 Reproduction of plane waves using a least squares approach

Using equation (2), one now seeks to generate a desired sound pressure field $\mathbf{p_t}$, defined as follows:

$$\mathbf{p_t} = [p_{t1}, p_{t2}, \ldots, p_{tm}, \ldots, p_{tM}]^T. \quad (6)$$

In our case, the target sound field p_{tm} is chosen as a plane wave of elevation ϕ and azimuth θ:

$$p_{tm} = e^{-jk(\sin\phi\ \cos\theta\, x_m + \sin\phi\ \sin\theta\, y_m + \cos\phi\, z_m)}. \quad (7)$$

The coordinates (x_m, y_m, z_m) correspond to the microphones' positions as shown in Figure 1.

The target pressure $\mathbf{p_t}$ is obtained by determining the different source strengths u_l. The problem is thus set to determine $\min_{\mathbf{u}} |\mathbf{p_t} - \mathbf{Gu}|_2^2$, that is, finding the weights $\mathbf{u_{opt}}$ that minimize the 2-norm of the squared error between the target sound pressure and the sound pressure radiated by the loudspeaker array at the microphone locations. When the system is overdetermined ($M > L$), an approximate solution can be obtained by the least squares method:

$$\mathbf{u_{opt}} = \left[\mathbf{G^H G} + \lambda \mathbf{I}\right]^{-1} \mathbf{G^H p_t}, \quad (8)$$

where $^\mathbf{H}$ denotes the conjugate transpose of a matrix. A regularization parameter λ is introduced to limit the magnitude of input signals of the loudspeaker array and to tackle situations where the condition number of $\mathbf{G^H G}$ is large (ill-conditioned problem).

The error ε between the target and reproduced sound fields is calculated as:

$$\varepsilon = \frac{|\mathbf{p_t} - \mathbf{Gu}|_2}{|\mathbf{p_t}|_2}. \quad (9)$$

2.3 Propagation over a sound absorbing material

This section introduces the porous material modeling within the framework of the Johnson–Champoux–Allard (JCA) [25] theory for a point source excitation. The principle of the two-microphone technique is also recalled in order to calculate the surface impedance Z_s of the material and its sound absorption coefficient α. The chosen test material is a polyurethane foam, whose parameters are listed in Table 1. These parameters were measured using a method [26] developed at Centre de Transfert de Technologie du Mans (CTTM). This method is based on the low frequency properties of an acoustic impedance sensor that allows assessing the complete fluid equivalent parameters of a porous material from a single test bench.

The sound pressure field created at point (r, z) by a point source located at (0, z_s) above a laterally infinite layer of porous material is calculated using an integral formulation [27, 28]:

Table 1. JCA model parameters of the polyurethane foam used in numerical simulations and experiments.

σ	10,000 (N·s·m^{-4})	Flow resistivity
h_p	0.05 (m)	Thickness of the porous layer
ϕ	0.93	Porosity
Λ	60 (μm)	Viscous characteristic length
Λ'	100 (μm)	Thermic characteristic length
α_∞	1.1	Tortuosity

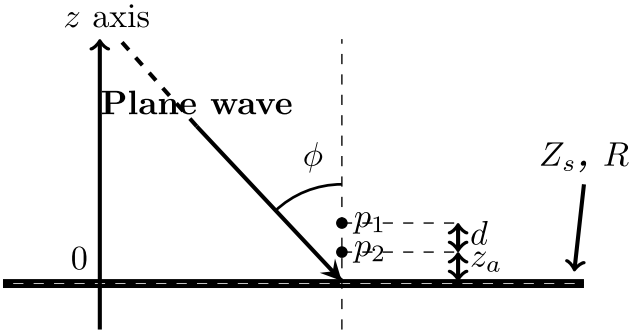

Figure 3. Diagram of the microphone pair with a plane wave incident on a sound absorbing plane of surface impedance Zs.

$$p(r,z) = u_l[g_{\text{inc}} + g_r], \quad (10)$$

$$g_{\text{inc}} = \frac{e^{-jk_0 r_1}}{r_1}, \quad (11)$$

$$g_r = -\frac{e^{-jk_0 r_2}}{r_2} - \int_0^\infty \frac{2\rho_1 e^{-\nu_0(z_l+z_m)}}{\rho_1 \nu_0 + \rho_0 \nu_1 \tanh \nu_1 h_p} k J_0(kr)\mathrm{d}k, \quad (12)$$

with $\nu_{i=0,1}^2 = k^2 - k_{i=0,1}^2$, where k_0 and k_1 are the wave numbers in the air and in the porous material, respectively, ρ_0 and ρ_1 are the air density and the porous material density, respectively, r_1 the source-microphone distance, r_2 the image source-microphone distance, J_0 is the cylindrical Bessel function of order 0, h_p the material thickness, z_l the loudspeaker height above the material surface, z_m the microphone height, r the source-microphone distance (projected on the material's surface) and u_l is the source strength. The wave number k_1 and density ρ_1 of the material are frequency-dependent, complex values obtained from the JCA model.

Assuming that the source array creates a perfect plane wave of incidence angle ϕ, the two-microphone technique [24] (Fig. 3) can be used to calculate the plane-wave reflection coefficient R from the ratio of the pressure signals measured by the two microphones ($H = p_2/p_1$):

$$R = \frac{H - e^{jk_0 z_a \cos\phi}}{e^{-jk_0 z_a \cos\phi} - H} e^{2jk_0 d\cos\phi}, \quad (13)$$

with ϕ the angle of the plane wave with respect to the normal of the material, d the inter-microphone separation and z_a the height of the nearest microphone with respect to the material.

The plane wave surface impedance Z_s and sound absorption coefficient α can then be deduced using:

$$Z_s = \frac{\rho_0 c_0}{\cos\phi}\frac{1+R}{1-R}, \tag{14}$$

and

$$\alpha = 1 - |R|^2, \tag{15}$$

with c_0 the speed of sound in air. The normalized surface impedance z_s is given by: $z_s = Z_s/(\rho_0 c_0)$.

3 Numerical simulations of plane wave reproduction in free-field

In this section, the results are obtained in free field condition, and the filter weights $\mathbf{u_{opt}}$ calculated from equation (8) are applied to the L point sources. The source array is a planar square array of side length $a = 105$ cm and is composed of 64 point sources. It is placed at a distance $h = 50$ cm above a planar square microphone array of side length $b = 60$ cm and composed of 81 sensors as depicted on Figure 1.

3.1 Reproduced sound pressure field

Figure 4 shows the reproduced plane wave with incidence angles $\theta = 50°$ and $\phi = 55°$, at a frequency of 1500 Hz in the xy and xz planes. The target wave is well reproduced in the plane of the microphones ($z = 0$). In the xz plane and for $y = 0$, the target wave is correctly reproduced in the region $z \lesssim 0.15$ cm where the reproduction error remains low. Figure 5 shows the error in the xz plane ($y = 0$) at 1500 Hz for various incidences. At low incidence, the target wave is well reproduced over a large area above the material. This area decreases greatly down to 1 or 2 cm above the targeted plane when grazing incidences are considered. This result is also frequency dependent: at low frequency the accurate reproduction area is larger than at high frequency. These results imply that the measurement of sound absorption with a microphone pair for high frequency and large incidences will be challenging, as both the material and the microphone pair are not in the error-free zone.

The reproduction error in the plane $z = 0$ is then averaged and plotted as a function of frequency in Figure 6. The inverse of the condition number and the average amplitude of the sources are also superimposed. Note that for the evaluation of ϵ in simulations, a grid twice as dense as the microphone grid, is used to better evaluate the actual error. This is the case for all simulated error plots in Sections 3 and 5. In simulations and despite a large condition number, with a low value of the regularization number $\lambda = 10^{-7}$, the reproduction error and the amplitudes of the sources remain low. The system is thus able to produce the desired sound field. At high frequencies (HF), when the reproduced wavelength becomes smaller than the loudspeaker spatial separation, the error increases significantly until reaching a value larger than 100%. These observations allow designing the measurement system for the targeted frequency range as detailed in the following section.

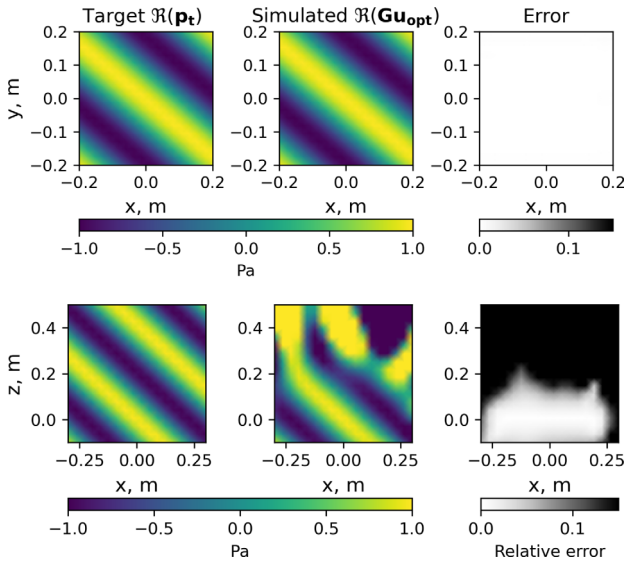

Figure 4. Real parts of the target and simulated sound pressure fields in the xy plane ($z = 0$) and xz plane ($y = 0$) at 1500 Hz for a plane wave of incidence $\phi = 55°$ and azimuthal angle $\theta = 50°$. The regularization parameter λ is equal to 10^{-5}. The error between target and simulated sound pressure fields is shown in the right column.

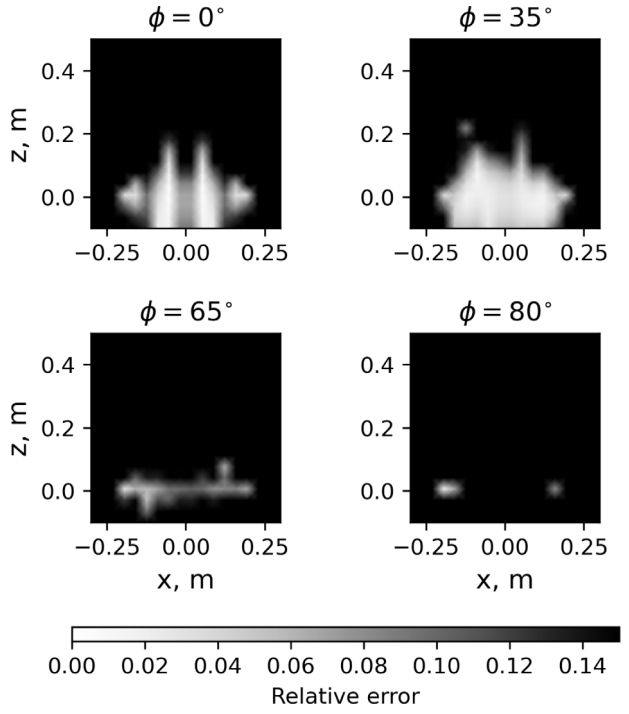

Figure 5. Error between target and simulated sound pressure fields in the xz plane ($y = 0$) at 1500 Hz for various plane wave incidences ϕ and for azimuthal angle $\theta = 50°$, with regularization parameter $\lambda = 10^{-5}$.

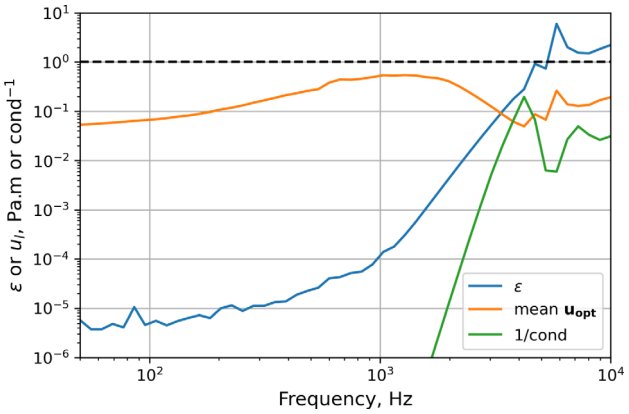

Figure 6. Reproduction error ε in the target plane xy, the inverse of condition number of the matrix $\mathbf{G}$ and average amplitude of the sources for the configuration shown in Figure 1.

3.2 Parametric study

In order to design the loudspeaker array following a target frequency range, numerical simulations are performed to investigate the influence of several parameters on the reproduced plane wave. The reference configuration is the one shown in Figure 1, one parameter is varied at a time while the others are kept constant.

3.2.1 Effect of varying microphone and source arrays dimensions

Figures 7a and 7b show the reproduction error ϵ in the reproduction plane when the sizes of the loudspeaker array (a) and the microphone array (b) are varied, respectively, while keeping the number of sources and microphones constant. The larger the source array size, the smaller the error at low frequencies (LF) while the upper cut-on frequency occurs earlier. The source amplitudes remain low while the target reproduction area is lower than the source array area. From Figure 7b, it appears that the smaller the microphone array size the smaller the error at LF while the cut-on occurs at higher frequencies. It should be noted that when b becomes larger than a, the optimal source amplitudes increase. It is indeed more difficult for the system to generate the target pressure over a large reproduction area with a small loudspeaker array.

3.2.2 Number of loudspeakers and microphones

Figures 7c and 7d show the reproduction error ε when the number (or density) of loudspeakers and microphones are varied respectively while the source array size $a = 105$ cm and microphone array size $b = 40$ cm are fixed. As expected, when the number of control microphones is equal to the number of loudspeakers the best reproduction error is obtained. Having more microphones than loudspeakers or the reverse does not increase the reproduction accuracy nor extend the frequency range of the system.

The source amplitudes remain low and mostly constant in the frequency range where the reproduction error is low. One can note that it is still possible to reach an acceptable result while using less microphones than loudspeakers.

3.2.3 Height of the loudspeaker array

Using the configuration shown in Figure 1, Figure 7e shows the reproduction error ε when the height h of the loudspeaker array above the target reproduction plane is varied. A larger loudspeakers to microphones separation leads to a larger error at LF, while the HF cut-on occurs earlier. This observation is only valid down to a 30 cm separation in this configuration. Below this value, the source amplitudes and reproduction errors start to increase again. When the sources are close to the control microphones, each microphone essentially picks up the sound radiation of the nearest source only. This error would also increase in practice as the near field of a loudspeaker does not follow the point source hypothesis. The source amplitudes also increase as h increases, this being explained by the $1/r$ sound pressure decrease with distance in free-field conditions.

3.2.4 Plane wave incidence angle

Finally, Figure 7f shows the reproduction error ε for different angles of incidence of the plane wave. As the angle of incidence increases, both the reproduction error and the amplitude of the sources increase. Indeed, the reproduction system is more suited for the reproduction of a wave propagating in a direction perpendicular to the material surface (the array of sources being parallel to the surface of the material and directly above the microphone antenna). Larger incidence angles are achievable but require more complex phase and magnitude relations between the different loudspeakers to generate the targeted sound field. The large source amplitudes observed at higher incidence in Figure 7f may induce concrete limitations (non-linear response of the loudspeakers, increase of unwanted reflections and diffraction effects from the environment or material edges). This point is further discussed in Section 5.4. Similarly, the cut-on frequency decreases as the angle of incidence increases, this can be observed when the error reaches a value of 0.1. Thus, if one wants to characterise the sample over the same frequency bandwidth at different elevation angles, it is mandatory to use the parametric levers presented here to tune the system.

3.2.5 Regularization parameter

A larger regularization parameter limits the loudspeaker amplitudes, resulting in a larger reproduction error. Overall, the regularization does not significantly modify results except below $\lambda = 10^{-9}$ where the regularization is not large enough to compensate for the ill-conditioning of the matrix $\mathbf{G}^{\mathbf{H}}\mathbf{G}$, which generates errors during its inversion. Note that the value of the regularisation parameter depends on the magnitude of the $\mathbf{G}$ matrix and cannot be generalised to any other configuration. For example, the value tuned for simulations with point sources cannot be matched with the value used in measurements. In order to generalise the λ value, one needs to establish a proper loudspeaker

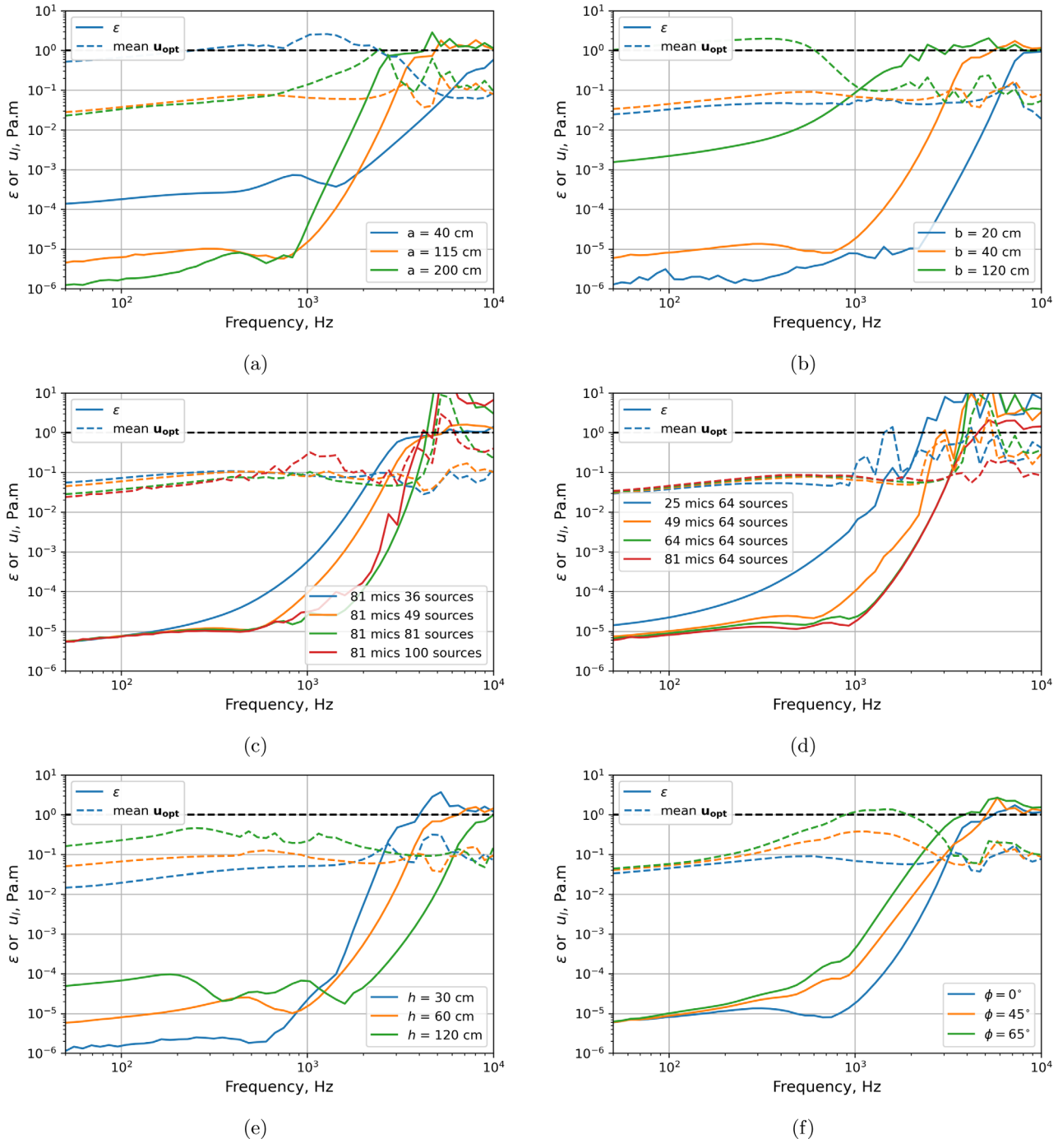

Figure 7. Reproduction error ε in the xy plane at $z = 0$ and mean amplitude $\mathbf{u}_{\mathbf{opt}}$ of the sources when varying a parameter of the system: Dimension of the source array a (a), Dimension of the microphone array b (b), number of sources Δ_l (c), number of microphones Δ_m (d), height of the loudspeaker array h (e), angle of incidence ϕ (f). The other parameters remain constant and are given in Figure 1.

modelling, correlating the amplitude of the loudspeakers to microphones Frequency Response Functions (FRF) between theory and experiments. This is however an unnecessary tedious process, especially when considering a measurement in free field condition, where the selection of λ is not critical as long as the system is well designed (a unique low value of λ can be used over the whole frequency range).

3.2.6 Parametric study summary

It was shown that a number of levers can be adjusted to properly size the sound field synthesis system. Indeed, depending on the targeted largest incidence angle and desired frequency bandwidth, the dimensions of the source and microphone arrays can be chosen to obtain the most

accurate reproduction results. Increasing the frequency bandwidth can be achieved by:

- decreasing the size a of the source array (leads to a higher cut-on frequency at the cost of a larger but reasonable reproduction error at low frequencies);
- decreasing the size b of the microphone array;
- increasing the number of sources and microphones;
- increasing the height of the sources above the microphone plane.

The easiest way to control the result is the size of the reproduction area as the other parameters cannot be changed once the measurement has been made. This means that we can consider only a subset of the microphone array in the reproduction process.

The inclusion of oblique incidence shows limiting behaviors and predisposes the system to operate with reduced precision when high incidences are considered.

With regard to the experimental implementation aiming for a frequency bandwidth of 100–4000 Hz while considering the loudspeaker array available, geometric parameters suggested in Figure 1 are adopted.

4 Simulation: sound field synthesis over a porous material

The previous system (Fig. 1) is now considered as positioned above an laterally infinite layer of porous material (see Sect. 2.3). The sound field above the material is derived from the computed input signals u_{opt} using equation (10). Figures 8a and 8b respectively show values of the sound absorption coefficient α and acoustic impedance z_s, both calculated using the two-microphone technique and for three different incidence angles. Simulated results are compared to the expected results, that are calculated from the JCA model. The sound absorption is well recovered at low frequencies although some small discrepancies with the theoretical results are observed. These discrepancies are more pronounced on the real part of the impedance, suggesting either a numerical problem or a residual effect of exponentially-decaying waves in the direction perpendicular to the material surface. At HF, it is observed that when the angle of incidence increases, the cut-on frequency in the reproduction error decreases. This can be directly related to the reproduction error of the sound field (see Fig. 3f). Interestingly, using the values of ϵ allows to establish beforehand the approximate HF limit of the measurement set-up.

In a second step, the same configuration is used, but a Gaussian random signal is added to the matrix of transfer functions $\mathbf{G}$ to reach a +50 dB signal to noise ratio (SNR). This aims to mimic the background noise observed during actual measurements of $\mathbf{G}$, or to illustrate the effect of a discrepancy between the theoretical $\mathbf{G}$ used in computations (theoretical point source propagation) and the actual $\mathbf{G}$ measured with loudspeakers.

The results for the configuration 1 are shown on Figures 9a, 9b, for the reproduction error ε, the sound absorption α and the normalized surface impedance z_s, respectively. The

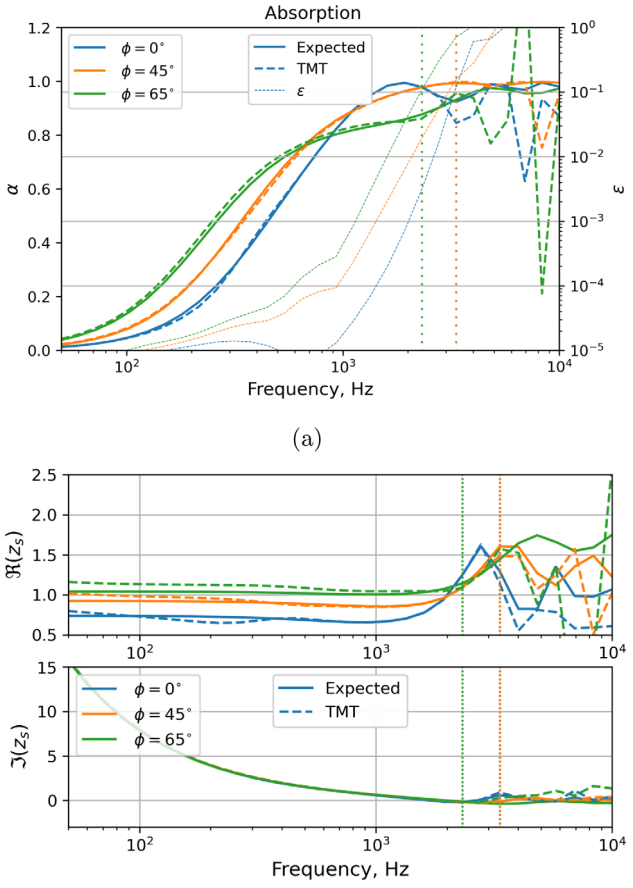

Figure 8. Absorption coefficient α and reproduction error ϵ (a), normalized surface impedance z_s (b), for the configuration shown in Figure 1 for three incidence angles with $a = 105$ cm, $b = 40$ cm, $\theta = 45°$, $\lambda = 10^{-7}$, $d = 2$ cm, $z_a = 0.5$ cm. Vertical dotted lines symbolise the estimated HF limit. TMT stands for Two-Microphone Technique.

reproduction error is largely increased at low frequencies (10^{-3} instead of 10^{-5} without noise). This error is not clearly translated into the sound absorption results but is visible on the real part of the estimated normalized surface impedance z_s below 100 Hz.

5 Experiments

This section discusses the experimental validation of the presented method. It is separated into two parts reflecting two different implementations of the method. The first one uses a full physical system consisting in 64 loudspeakers. The second uses a system moving a single loudspeaker with a robot to perform sequential measurements that are summed afterwards to recreate the sound field that would be reproduced by a real array. For the experimental part, the elements of the matrix $\mathbf{G}$ of equation (4) now correspond to transfer functions between a given loudspeaker and a given microphone and are therefore expressed in Pa/V. Consequently, the source strengths u_l are described by the loudspeaker input voltages and expressed in volts.

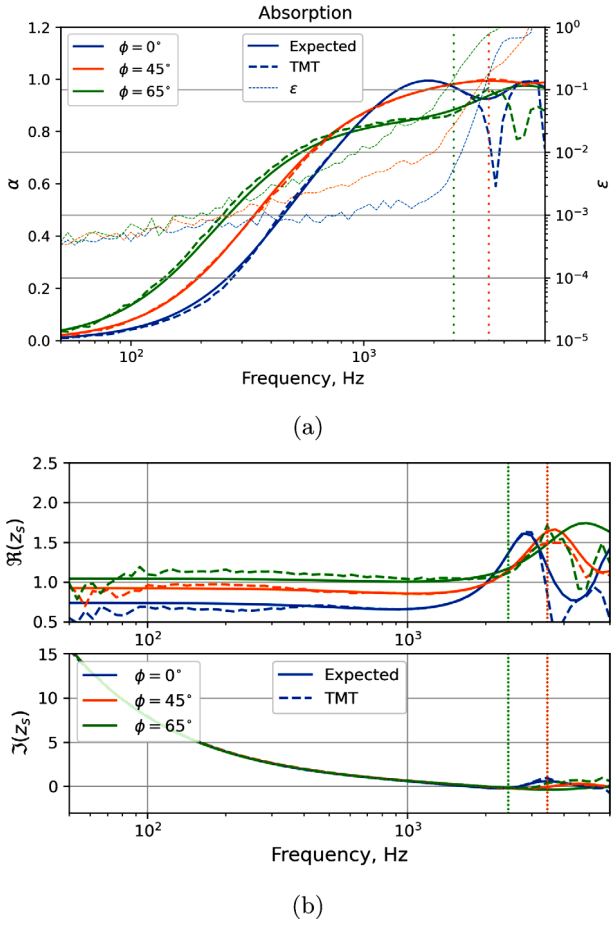

Figure 9. Absorption coefficient α and reconstruction error (a), normalized surface impedance z_s (b), for the configuration shown in Figure 1 for three incidence angles with $a = 105$ cm, $b = 40$ cm, $\lambda = 10^{-7}$, $d = 2$ cm, $z_a = 0.5$ cm and added noise.

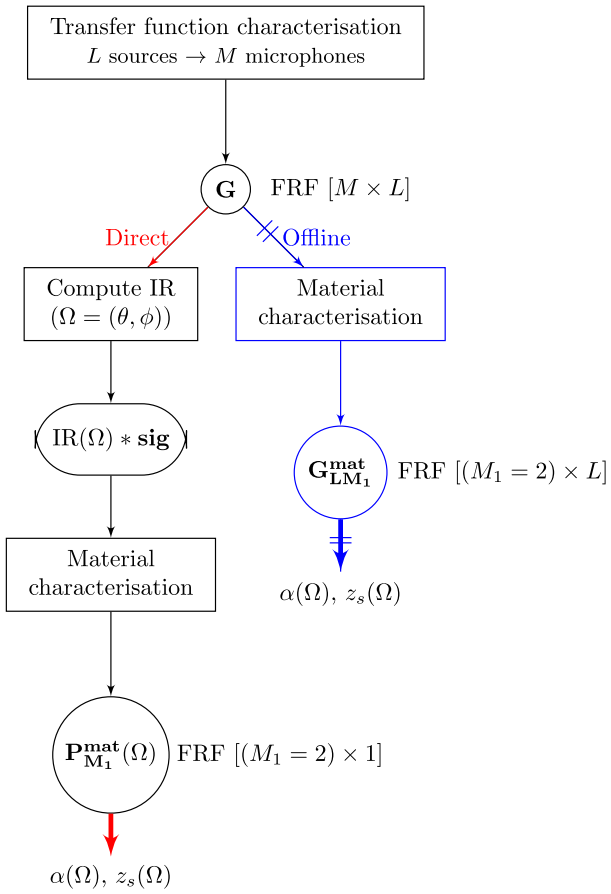

Figure 10. Block diagram of the experimental implementation of the full physical array.

5.1 Full physical setup

The system is shown in Figure 2. It consists in 64 Faital-PRO 3FE22 loudspeakers which are powered by 16 four-channels amplifiers (HPA D604). The amplifiers are driven by two RME-32DA converters that are both synchronized by a Madiface XT audio interface linked to a computer. The recording part is handled using the same Madiface board which also controls a RME-16AD analog to digital converter connected to a B&K Nexus amplifier and either a single or a pair of 1/4″ microphones. The sample is a 150 cm by 150 cm polyurethane foam panel, whose parameters are listed in Table 1 (see Sect. 2.3).

The experimental process is summarized in the block-diagram depicted in Figure 10, which shows that experiments can be conducted in two ways: a direct measurement with the 64 loudspeaker array or an offline measurement using previously measured FRF between reproduction loudspeakers and control microphones. Both methods require the measurement of the plant matrix $\mathbf{G}$ on a hard ground (assumption of a rigid surface). The experimental matrix $\mathbf{G}$ is used to compensate for the differences in loudspeaker sensitivities as well as for the intrusiveness of the system and also takes into account the fact that the loudspeakers do not strictly behave as point sources. The loudspeakers to microphones FRF are measured with microphones placed on the ground, in the absence of absorbing material. It is assumed that the sound pressure on the hard ground is twice that in a free field situation (pressure doubling hypothesis). This measurement is performed sequentially with a robot moving the same microphone along the desired grid of M points, as shown in Figure 2. This avoids microphone calibration issues but at the cost of a longer measurement time. Note that when the material to be tested is in position, the measurement is conducted with the system raised by a height corresponding to the thickness of the material, in order to reproduce the same target incident pressure field on the material surface.

In the direct approach, the optimal source inputs u_{opt} given by equation (8) in the frequency domain are inverse Fourier transformed to provide impulse response filters for the desired angles (θ, ϕ); these impulse responses are convoluted with a sweep signal (**sig**) to obtain the set of loudspeaker signals to be played by the system above a material. The signals recorded at two microphones (spaced here by $d = 3$ cm) are then used to determine $H = p_2/p_1$ for each frequency, and finally calculate $\alpha(\theta, \phi)$ and $z_s(\theta, \phi)$ from equations (13) to (15).

In the offline approach, the matrix $\mathbf{G}_{\mathbf{LM}}^{\mathbf{mat}}$ of FRF between each loudspeaker position and the microphone pair above the material is recorded for all loudspeakers of the full array. These data are used to calculate $\mathbf{P}_{\mathbf{M_1}}^{\mathbf{mat}} = \mathbf{G}_{\mathbf{LM_1}}^{\mathbf{mat}}\mathbf{u}_{\mathbf{opt}}$ at a post-processing phase for any incidence angle, where $\mathbf{u}_{\mathbf{opt}}$ is still obtained from equation (8). This enlarges post-processing possibilities (any $\alpha(\theta,\phi), z_s(\theta,\phi)$ can be derived from $\mathbf{G}_{\mathbf{LM}}^{\mathbf{mat}}$ matrices) but at the cost of a longer measurement time. Note that the single-source implementation, detailed in Section 5.6, also allows independent measurement of $\mathbf{G}_{\mathbf{LM}}^{\mathbf{mat}}$ and $\mathbf{G}$.

It has been observed that the offline and direct methods lead to almost the same results. However, the direct method is slightly more accurate in low frequencies, as it has a higher signal-to-noise ratio because all the loudspeakers operate at the same time. On the other hand, the offline method offers more post-processing possibilities and is more adapted to the research context of this article. It is possible to vary the number of control microphones in the calculation of $\mathbf{u}_{\mathbf{opt}}$, to change the angle of incidence θ or the azimuth angle ϕ without repeating the measurement.

The plant matrix $\mathbf{G}$ measurement on a hard ground consists in two averaged sweeps of around 8 s (50–7000 Hz) for each of the 64 loudspeakers, over two grids of microphone positions on the ground (10×10, $b = 60$ cm or 9×9, $b = 40$ cm). Since the microphone has to be sequentially translated by a robot, this measurement can take up to 10 hours depending on the desired microphone grid. Once the plant matrix $\mathbf{G}$ measurement is performed, the measurement of transfer functions between each loudspeaker and each microphone of the two-microphone probe over a material layer $\mathbf{G}_{\mathbf{LM}}^{\mathbf{mat}}$ takes about 20 min.

5.2 Perpendicular incidence results

All the following results were computed with the offline approach. Figure 11 shows the sound absorption and normalized surface impedance results obtained with the system shown in Figure 2 for perpendicular incidence. The sound absorption is well estimated from 100 Hz to 2000 Hz, with results close to those obtained with an impedance tube or using a JCA model. The high frequency limit corresponds to a reproduction error ε of around 10%, which is consistent with observations from simulations.

The measured reproduction errors (named $\varepsilon^{\text{meas}}$), calculated using equations (8) and (9) and the measured versions of matrix $\mathbf{G}$, are in good agreement with the theoretical errors (named ε^{th}) only above 1000 Hz. Below this frequency, the discrepancy is mostly due to measurement noise and the value of the regularization parameter λ chosen in the measurement.

Although α is well recovered, from 100 Hz to 200 Hz, discrepancies are observed, especially on the z_s curve. We hypothesize that these discrepancies are due to diffraction by the material edges, room modes or reflections, the measurement being particularly sensitive to low frequency disturbances because of the very low particular velocity existing close to a rigid boundary. Below 100 Hz, microphone calibration errors, poor loudspeaker efficiency and noise lead to unreliable results. Below 200 Hz, the reliability of the JCA model can also be questioned when comparing it to the impedance tube results, especially for the real part of z_s.

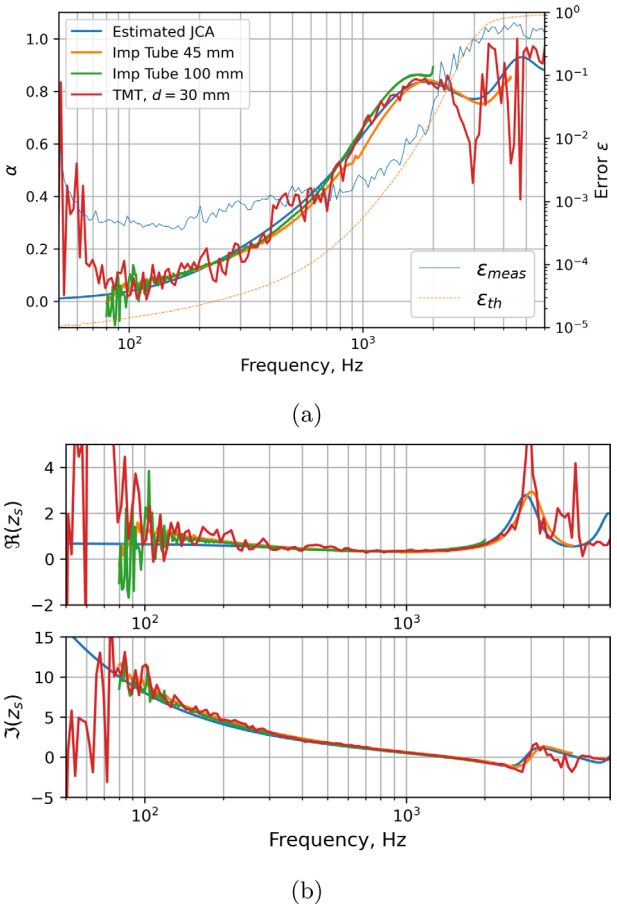

Figure 11. Absorption coefficient α and reproduction error ε (a), normalized surface impedance z_s (b), for the configuration shown in Figure 2 at normal incidence with $a = 105$ cm, $b = 60$ cm, $\Delta_m \approx 6.6$ cm, $\theta = 0°$, $\phi = 0°$, $z_a = 0.5$ cm, $d = 1.5$ cm. ϵ_{th}: $\lambda = 10^{-7}$, ϵ_{meas}: $\lambda = 0$.

5.3 Effect of the size of the target reproduction area

To complete the previous results, Figure 12 shows the absorption and normalized surface impedance of the system shown in Figure 2 at normal incidence while reducing the size of the target reproduction area b from 60 cm in Figure 11 down to 20 cm. To do so, the 9×9 microphone grid ($b = 60$ cm) is reduced by keeping the 5×5 central grid ($b = 20$ cm). As observed in the simulations, this increases the upper limit of the frequency range up to around 6000 Hz. An error in the estimation of α is observed at 3000 Hz. This was observed for several sets of data with this implementation of the system, a possible source of this problem is the microphone holder. The experimental reproduction error $\varepsilon_{\text{meas}}$ is out of range since in this case there are less microphones than loudspeakers. However, as shown in the simulations 3.2.2, it is still possible to obtain a solution from an under-determined system using a proper regularisation.

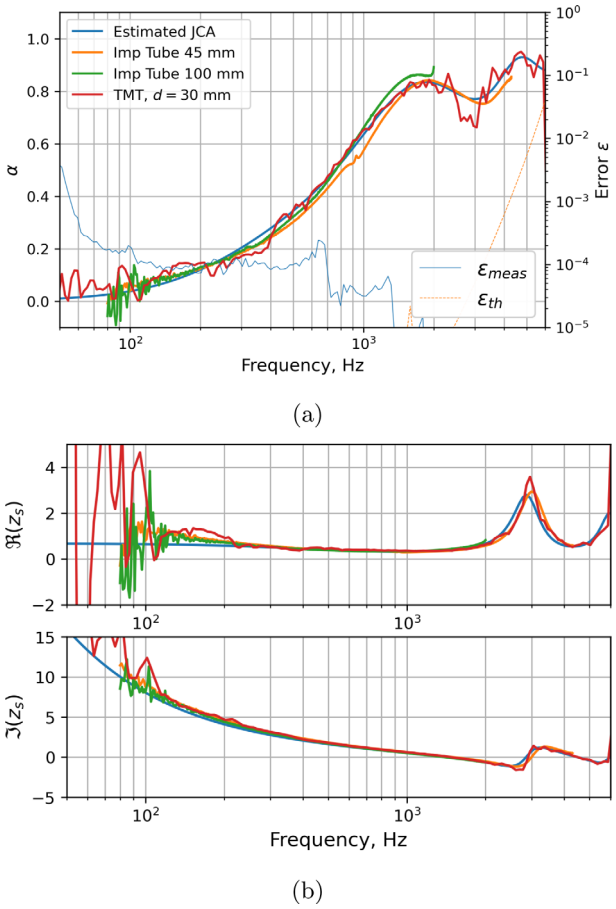

Figure 12. Absorption coefficient α and reproduction error ϵ (a), normalized surface impedance z_s (b), for the configuration shown in Figure 2 at normal incidence with $a = 105$ cm, $b = 20$ cm, $\Delta_m = 5$ cm, $\theta = 45°$, $\phi = 0°$, $\lambda = 10^{-7}$, $z_a = 0.5$ cm, $d = 1.5$ cm. ϵ_{th}, ϵ_{meas}: $\lambda = 10^{-7}$.

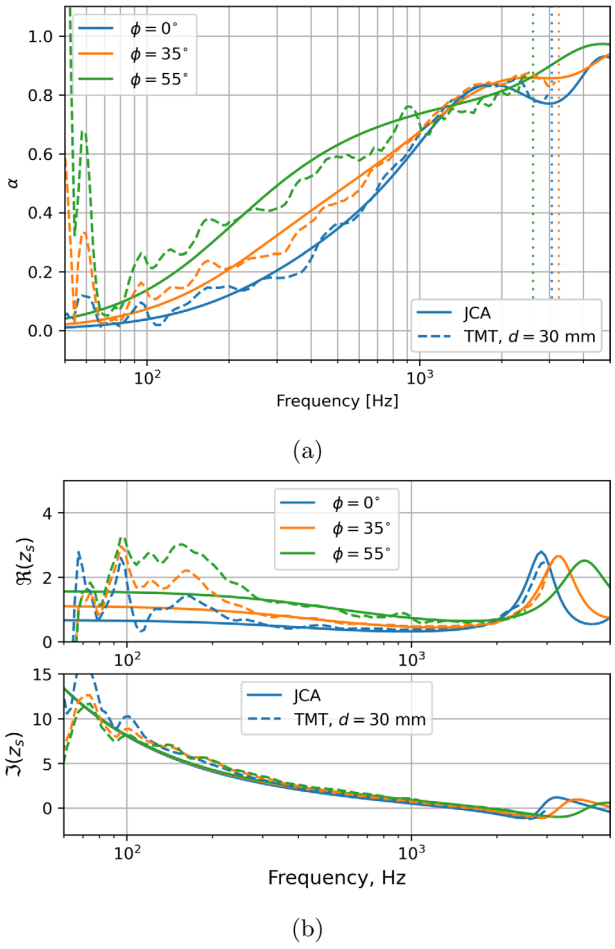

Figure 13. Absorption coefficient α (a), normalized surface impedance z_s (b), for the configuration shown in Figure 2 for three incidence angles with $a = 105$ cm, $b = 33$ cm, $\Delta_m \approx 6.6$ cm, $\lambda = 10^{-7}$, $z_a = 0.5$ cm.

5.4 Effect of the incidence angle

Figure 13 shows the sound absorption and normalized surface impedance results for three incidence angles, using the system shown in Figure 2. The obtained results for the sound absorption coefficient are consistent with predictions derived from the JCA model in the 300–2500 Hz frequency band for each incidence angle. Below 300 Hz, discrepancies with the JCA model are noticeable but calculations are based on parameters obtained from impedance tube measurements [26] (i.e. normal incidence, and on a small sample). Possible anisotropy of the material is not taken into account in impedance tube measurements and the trustfulness of the JCA model for large incidence angles is questionable. These reference curves should be taken as guidelines rather than ground truth. It is especially true concerning the surface impedance, for which the JCA model already showed differences with impedance tube results (see Sect. 5.2). It can also be noticed that as the incidence angle increases, oscillations due to unwanted reflections occur in the absorption curves (this is especially noticeable for the 55° incidence). A possible explanation is that when the reproduction of a target sound pressure field with grazing incidence is sought, larger loudspeaker inputs are required (see Sect. 3.2.4). This increase of the mean value and variance of the source amplitudes triggers imperfections in the reproduction system. Indeed, for a similar sound pressure level and for perpendicular incidence, larger source amplitudes will also induce stronger parasitic reflections which will lead to a very limited "error-free" reproduction zone above the control plane (see Sect. 3.1). The reproduction errors at the microphone pair will bias the estimation of the reflection coefficient R. Moreover, R is related to the surface impedance which depends on the perpendicular component of the acoustic velocity. At oblique incidence, the projection of the acoustic velocity onto the normal is small and sensitive to reproduction errors and measurement noise.

5.4.1 Azimuth averaging

The proposed approach allows modifying the azimuth direction θ of the incoming plane wave (in particular for the offline processing). The results should be invariant for

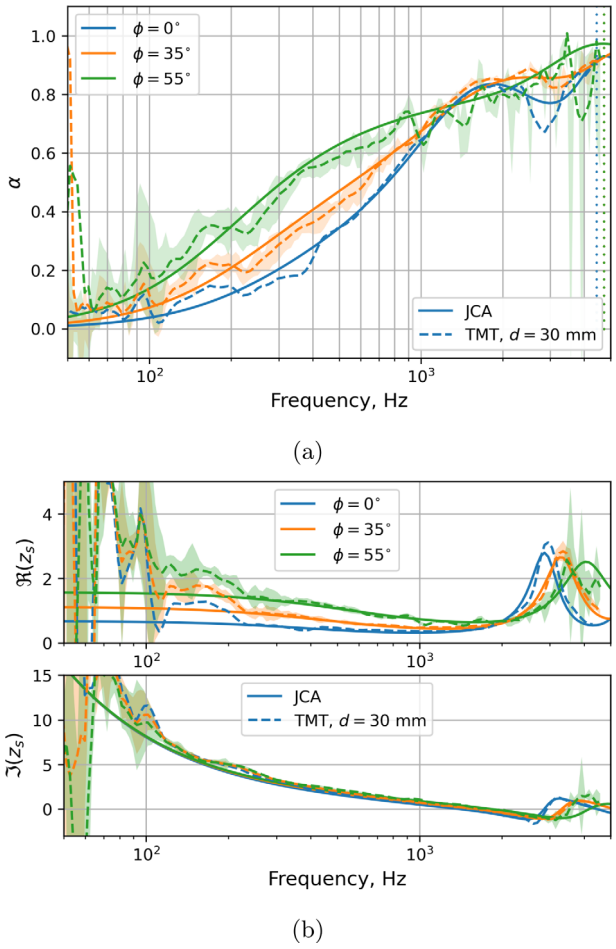

Figure 14. Mean absorption coefficient α (a), mean normalized surface impedance z_s (b), calculated with 20 azimuth angles $\theta \in [0, 2\pi]$ for three incidence angles ϕ and for the configuration shown in Figure 2 with $a = 105$ cm, $b = 33$ cm, $\Delta_m \approx 6.6$ cm, $\lambda = 10^{-9}$, $z_a = 0.5$ cm, $d = 3$ cm. The shaded areas indicate the variance of $\theta \in [0, 2\pi]$.

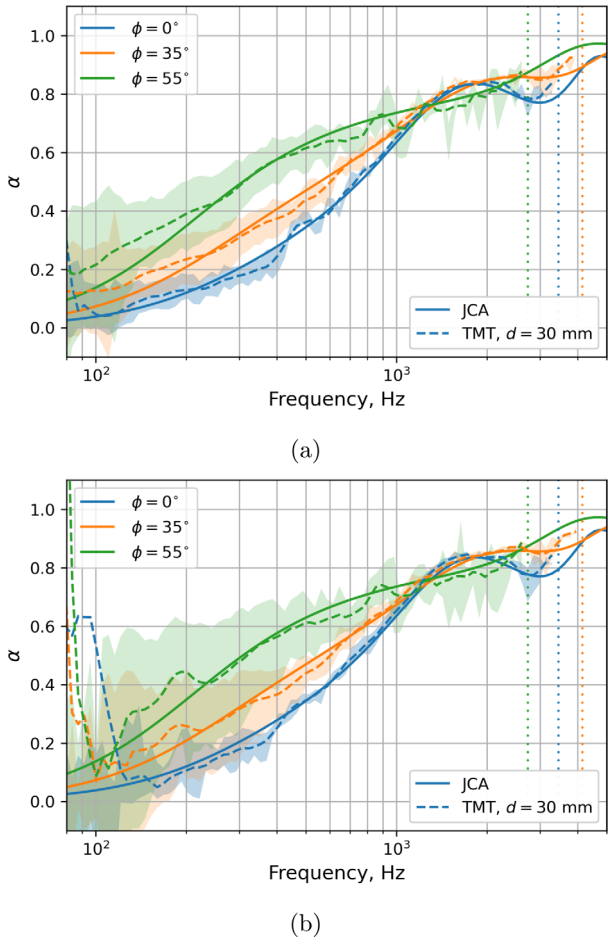

Figure 15. Averaged absorption coefficient α for different incidence angles ϕ for the configuration shown in Figure 2, with $a = 105$ cm, $b = 33$ cm, $\Delta_m \approx 6.6$ cm, $\lambda = 10^{-9}$, $z_a = 0.5$ cm, $d = 3$ cm. The shaded area shows the variance over 7 values of $\theta \in [0, 2\pi]$ and over 9 positions of a regular grid of size 4 cm × 4 cm (a) or 20 cm × 20 cm (b).

homogeneous infinite materials. Under practical conditions, both the imperfections of the loudspeaker array, the inhomogeneity and the finite size of the material lead to azimuth dependent results. Figure 14 shows the sound absorption and normalized surface impedance results of the system for different incidence angles averaged over twenty θ values $\in [0, 2\pi]$ with their associated variance. It can be observed that even if the various azimuth directions θ lead to different results, their variance remains limited above 150 Hz. The variance in α and z_s appears to be significantly larger for larger incidences ϕ.

5.5 Homogeneity in the target reproduction region

This section briefly investigates the spatial homogeneity of the reproduced sound pressure field. The two-microphone probe is moved over nine positions of a regular horizontal grid of size 4 cm × 4 cm. Figure 15a shows the sound absorption and the associated variance averaged over the grid points and over 7 values of $\theta \in [0, 2\pi]$. Figure 15b plots the same data but for a grid of 20 cm × 20 cm. For the small grid, the results are quite homogeneous especially for low incidence angles. On the other hand, for the large grid, the standard deviation is much larger although the average value of the measured absorption coefficient remains valid down to 200 Hz.

5.6 Sequential measurement

Instead of using the full system set-up, it is also possible to use a single loudspeaker which is moved sequentially with a robot. Since this system is less intrusive than a full loudspeaker array and under the assumption that the loudspeaker behaves as a point source, the calibration phase (measurement of $\mathbf{G}$) can be omitted. Only the transfer functions $\mathbf{G}_{\mathbf{LM}}^{\mathbf{mat}}$ between the single loudspeaker moved at successive positions and the microphone pair are thus measured above the material, which takes around 40 minutes using 2 averaged sweep of 8 s duration. The matrix $\mathbf{G}$ is computed under the assumption of theoretical point sources

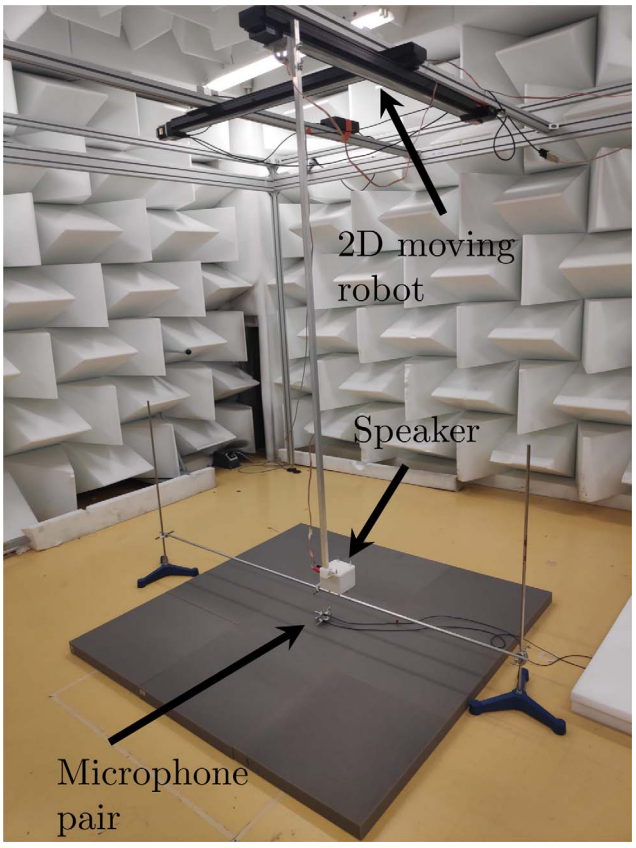

Figure 16. Picture showing the experimental set-up with a single mobile loudspeaker.

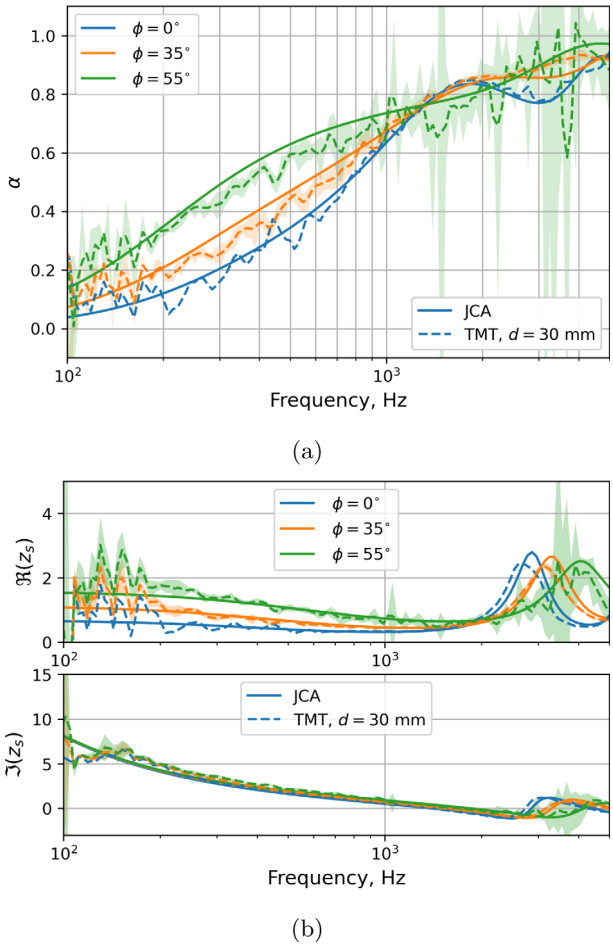

Figure 17. Absorption coefficient α (a) and normalized surface impedance z_s (b) for the system shown in Figure 16 for different incidence angles with $a = 100$ cm, $b = 20$ cm, $\Delta_m \approx 2$ cm, $\lambda = 10^{-7}$, $z_a = 0.5$ cm.

in a free field condition (Eq. (11)). The side length of the virtual array a had to be shortened from 105 to 100 cm due to a limited operating range of the robot.

Figure 17 shows the sound absorption and normalized surface impedance results of the system shown in Figure 16 for different incidence angles averaged over 20 azimuth angles $\theta \in [0, 2\pi]$. The variance of the results is also plotted. As previously, the results show a good agreement with the theory between 150 and 5000 Hz. Below 150 Hz the results are biased, because of the low signal to noise ratio, limits of the point source hypothesis (near-field effect in the Fresnel zone) and possible calibration problems as two microphones are used for the calculation of H (albeit they where relatively calibrated, light alteration of the sensitivity in LF can lead to strong deviation in the measurements).

In HF, discrepancies with the JCA predictions are observed for large incidence angles, see for instance the results for $\phi = 55°$ in Figure 17. The standard deviation shown by the green shaded area around the solid line in Figure 17 is much larger than with the full system (Fig. 14a). This is attributed to the mismatch of the point source assumption with reality, the loudspeakers being more directive at higher frequency and to the fact that the side speakers have a higher amplitude for large incidence angles. When comparing the direct and offline methods to the expected results, it appears that the point source assumption remains acceptable, especially for frequencies below 1000 Hz or when the incidence is lower than 45°.

5.7 Full setup versus sequential measurement

The use of a full reproduction system (L loudspeakers) involves:

- A tedious calibration phase, that could be however fully automatized and optimized;
- Fast measurement once the system is calibrated;
- A larger signal to noise ratio by summing the contribution of L loudspeakers;
- A larger complexity and cost (L loudspeakers all independently wired and driven);
- The loudspeaker positions in the array are currently fixed, and it is not easy to change them quickly.

The use of a sequential system involves:

- A minimal setup including two microphones, one loudspeaker, a 2D displacement robot and associated electronics and wiring;
- No calibration phase, except for the microphone pair;
- Less diffraction effects;
- The dimensions of the virtual loudspeaker array can be easily modified.

Thus, from a practicality point of view the sequential system is much easier to implement, while the full system allows very fast measurements once it is set up and calibrated.

6 Conclusion

This article presented a sound field synthesis method for characterizing acoustic materials under plane wave excitation at arbitrary incidence angle. In the literature, similar implementations only provided results at normal incidence and for a limited frequency bandwidth (250–1600 Hz). A comprehensive parametric analysis of the system was first performed, showing how to design the system in order to achieve a target frequency bandwidth. A simple criterion can be used to evaluate the HF cut-on frequency, and is based on the expected reproduction error. The method was then tested on a 150 cm × 150 cm sample of polyurethane foam (this area being relatively small compared to the reverberation chamber standard requirement). Sound absorption α and normalized surface impedance z_s were well estimated between 100 Hz and 5000 Hz for normal incidence and showed a good agreement with the JCA modeling. For oblique incidence, the effective frequency range is decreased to 100 Hz – 3000 Hz at 55° incidence angle. Two different implementations of the system were tested: a full system consisting of 64 loudspeakers and a sequential system with a robotized single loudspeaker. The full system allows fast measurements once calibration is done, with improved results at high frequency compared to the sequential system. The latter nevertheless offers a much simpler installation and operation. Several points need further investigations: effect of the material size (thickness and side length), influence of the room reverberation. As the presented method allows to characterize a material at all incidence angles, the reconstruction of the diffuse field absorption by analogy with the reverberation room method is planned in the future. To enlarge the low frequency range, the use of a loudspeaker with a lower cut-on frequency in combination with a moving microphone will be considered to increase the SNR and limit the calibration error.

Conflict of interest

The authors declare no conflict of interest.

Acknowledgments

This work was conducted within the framework of the "Centre Acoustique Jacques Cartier'', an International Research Project labeled by the Centre National de la Recherche Scientifique (CNRS). The authors thank Nicolas Poulain at CTTM for performing the measurements used to obtain the parameters of the JCA model, James Blondeau and Félix Lebeuf for their help with the measurements.

References

1. ASTM E150–12: Standard test method for impedance and absorption of acoustical materials using a tube, two microphones and a digital frequency analysis system. American Society for Testing Material International, 2012.
2. ISO 10534–2: Acoustics – Determination of sound absorption coefficient and impedance in impedance tubes – Part 2: Transfer-function method. International Organization for Standardization, 1998.
3. ISO 354: Acoustics – Measurement of sound absorption in a reverberation room. International Organization for Standardization, 2003.
4. ASTM C423–09a: Standard test method for sound absorption and sound absorption coefficients by the reverberation room method. American Society for Testing Material International, 2009.
5. M. Vercammen: Improving the accuracy of sound absorption measurement according to ISO 354, in Proceedings of the International Symposium on Room Acoustics, Melbourne, Australia, 2010.
6. C.-H. Jeong, J.-H. Chang: Reproducibility of the random incidence absorption coefficient converted from the sabine absorption coefficient. Acta Acustica united with Acustica 101 (2015) 99–112.
7. J.F. Allard, Y. Champoux: *In situ* two-microphone technique for the measurement of the acoustic surface impedance of materials. Noise Control Engineering Journal 32 (1989) 15–23.
8. R. Lanoye, G. Vermeir, W. Lauriks, R. Kruse, V. Mellert: Measuring the free field acoustic impedance and absorption coefficient of sound absorbing materials with a combined particle velocity-pressure sensor. Journal of the Acoustical Society of America 119 (2006) 2826–2831.
9. J. Ducourneau, V. Planeau, J. Chatillon, A. Nejade, Measurement of sound absorption coefficients of flat surfaces in a workshop, Applied Acoust. 70 (2009) 710–721.
10. W.-L. Lin, C.-X. Bi, M. Vorländer, Y.-B. Zhang, R. Opdam: *In situ* measurement of the absorption coefficient based on a time-domain subtraction technique with a particle velocity transducer. Acta Acustica united with Acustica 102 (2016) 945–954.
11. K. Hirosawa, K. Takashima, H. Nakagawa, M. Kon, A. Yamamoto, W. Lauriks: Comparison of three measurement techniques for the normal absorption coefficient of sound absorbing materials in the free field. Journal of the Acoustical Society of America 126 (2009) 3020–3027.
12. T. Otsuru, R. Tomiku, N.B.C. Din, N. Okamoto, M. Murakami: Ensemble averaged surface normal impedance of material using an in-situ technique: Preliminary study using boundary element method. Journal of the Acoustical Society of America 125 (2009) 3784–3791.
13. E. Brandão, A. Lenzi, J. Cordioli: Estimation and minimization of errors caused by sample size effect in the measurement of the normal absorption coefficient of a locally reactive surface. Applied Acoustics 73 (2012) 543–556.
14. A. Richard, E. Fernandez-Grande: Comparison of two microphone array geometries for surface impedance estimation. Journal of the Acoustical Society of America 146 (2019) 4115–4125.
15. M. Nolan, S. Verburg, J. Brunskog, E. Fernandez-Grande: Experimental characterization of the sound field in a reverberation room. Journal of the Acoustical Society of America 145 (2019) 2237–2246.
16. S. Dupont, M. Melon, A. Berry: Characterization of acoustic material at oblique incidence using a spherical microphone array. Journal of the Acoustical Society of America 147 (2020) 3613–3625.

17. M. Nolan: Estimation of angle-dependent absorption coefficients from spatially distributed *In situ* measurements. Journal of the Acoustical Society of America 147 (2020) EL119–EL124.
18. O. Robin, A. Berry, O. Doutres, N. Atalla: Measurement of the absorption coefficient of sound absorbing materials under a synthesized diffuse acoustic field. Journal of the Acoustical Society of America 136 (2014) EL13–EL19.
19. O. Robin, C. Amedin, A. Berry, N. Atalla, O. Doutres, F. Sgard: Assessing sound absorption coefficient under a synthetized diffuse acoustic field: effect of the sample size and nature, in Proceedings of Internoise, 9–15 August 2015, San Francisco, CA, USA, 2015.
20. O. Robin, A. Berry, S. Moreau: Experimental synthesis of spatially-correlated pressure fields for the vibroacoustic testing of panels. Flinovia – Flow Induced Noise And Vibration Issues And Aspects (2015) 151–185.
21. O. Robin, A. Berry, C. Kafui Amédin, N. Atalla, O. Doutres, F. Sgard: Laboratory In situ sound absorption measurement under a synthetized diffuse acoustic field. Building Acoustics 26 (2019) 223–242.
22. Y. Zhang, Z. Kuang, M. Wu, J. Yang: In-situ measurement of sound absorbing properties using plane-wave sound field reproduced by virtual loudspeaker array. Building and Environment 94 (2015) 883–890.
23. Y. Zhang, S. Tan, Z. Kuang, M. Wu, J. Yang: Measurement of sound absorbing properties under a plane-wave sound field reproduced by linear loudspeaker array, in 23rd International Congress on Sound & Vibration, Athens, Greece, 10–14 July 2016.
24. J.F. Allard, B. Sieben: Measurements of acoustic impedance in a free field with two microphones and a spectrum analyzer. Journal of the Acoustical Society of America 77 (1985) 1617–1618.
25. J.F. Allard, N. Atalla: Propagation of sound in porous media: modelling sound absorbing materials. Wiley, 2009.
26. J. Le Roux, J. Dalmont, N. Poulain: A new device for fluid equivalent parameters assessment, Symposium on the Acoustics of Poro-Elastic Materials (SAPEM), Online, March 29th–April 2nd 2021..
27. J.F. Allard, W. Lauriks, C. Verhaegen: The acoustic sound field above a porous layer and the estimation of the acoustic surface impedance from freeâfield measurements. Journal of the Acoustical Society of America 91 (1992) 3057–3060.
28. S. Thomasson: Sound propagation above a layer with a large refraction index. Journal of the Acoustical Society of America 61 (1977) 659–674.

Cite this article as: Dupont S. Sanalatii M. Melon M. Robin O. Berry A, et al. 2022. Characterization of acoustic materials at arbitrary incidence angle using sound field synthesis. Acta Acustica, **6**, 61.